Supplement of Atmos. Chem. Phys., 23, 10255–10265, 2023
https://doi.org/10.5194/acp-23-10255-2023-supplement

Atmospheric Chemistry and Physics Open Access

Supplement of

Influence of acidity on liquid–liquid phase transitions of mixed secondary organic aerosol (SOA) proxy–inorganic aerosol droplets

Yueling Chen et al.

Correspondence to: Zhibin Wang (wangzhibin@zju.edu.cn)

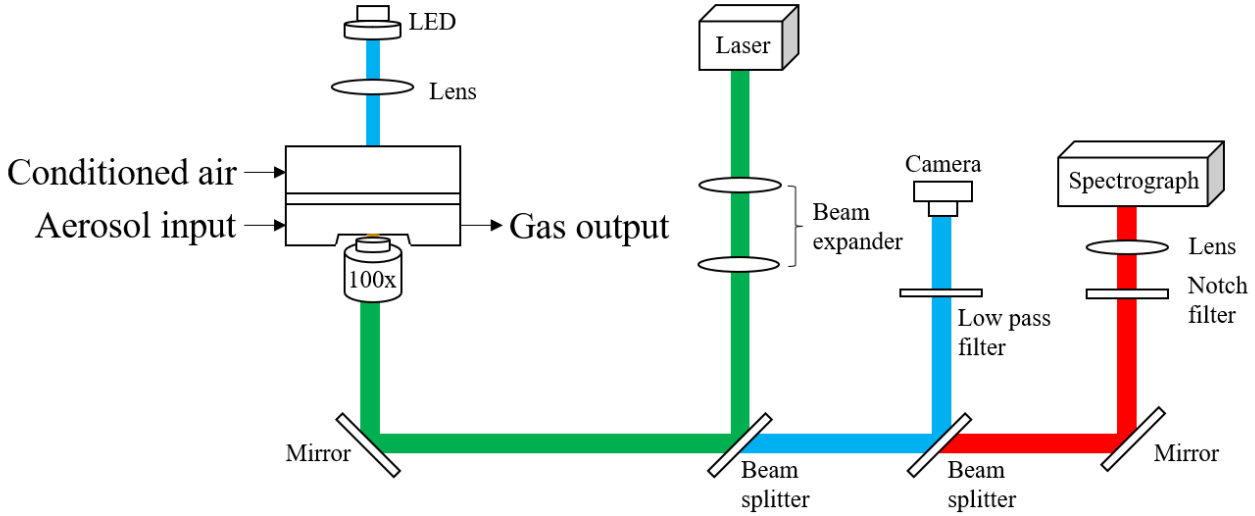

Figure S1. Schematic of aerosol optical tweezer setup used in this study. Medical nebulizer nebulized dissolved solution to generate aerosol droplets. Conditioned airflow is mixed by a dry airflow and a humid airflow that humidified by a water bubbler. A temperature and humidity sensor measured the temperature and RH of the conditioned airflow after it enters the chamber.

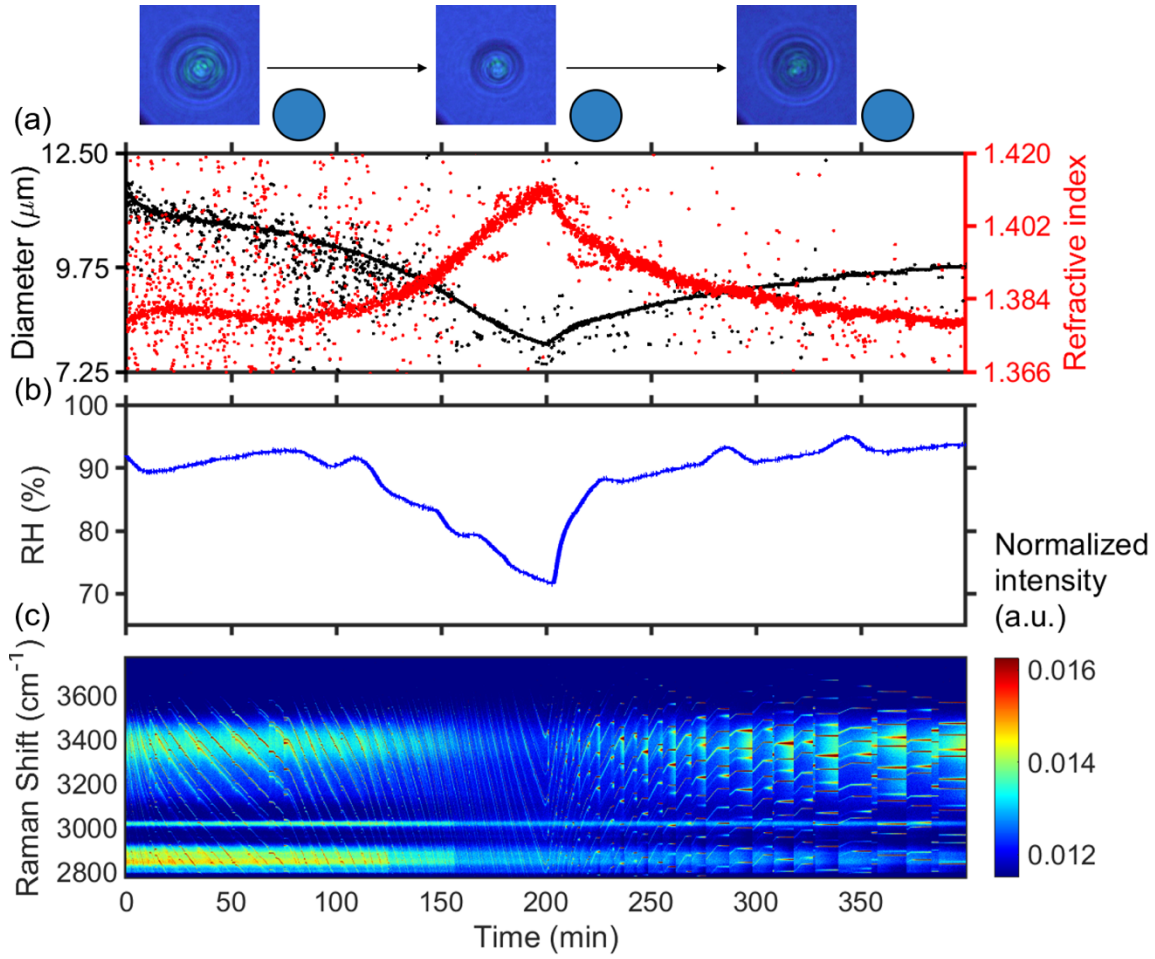

Figure S2. Result of GL/AS system. (a) Timescale of changes in droplet size and refractive index, determined from fitting the Raman shift positions of the WGMs. (b) RH variation after the trapping chamber during the humidity changing process with time. (c) Time-resolved Raman spectra.

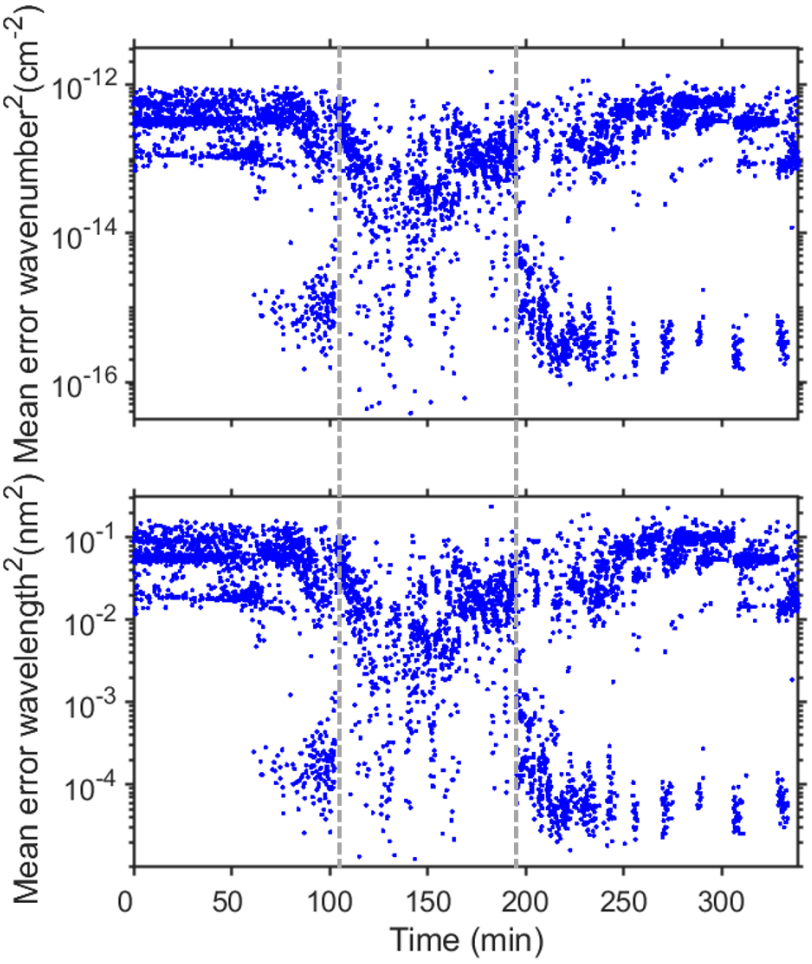

Figure S3. Fitting errors of the WGMs based on the homogenous Mie scattering model, corresponding to Figure 2 in the main text. The grey dashed lines indicated the moments of LLPS and phase mixing, respectively. The messy points in the figure primarily resulted from the errors generated during the batch peak finding process using the ipeak algorithm.

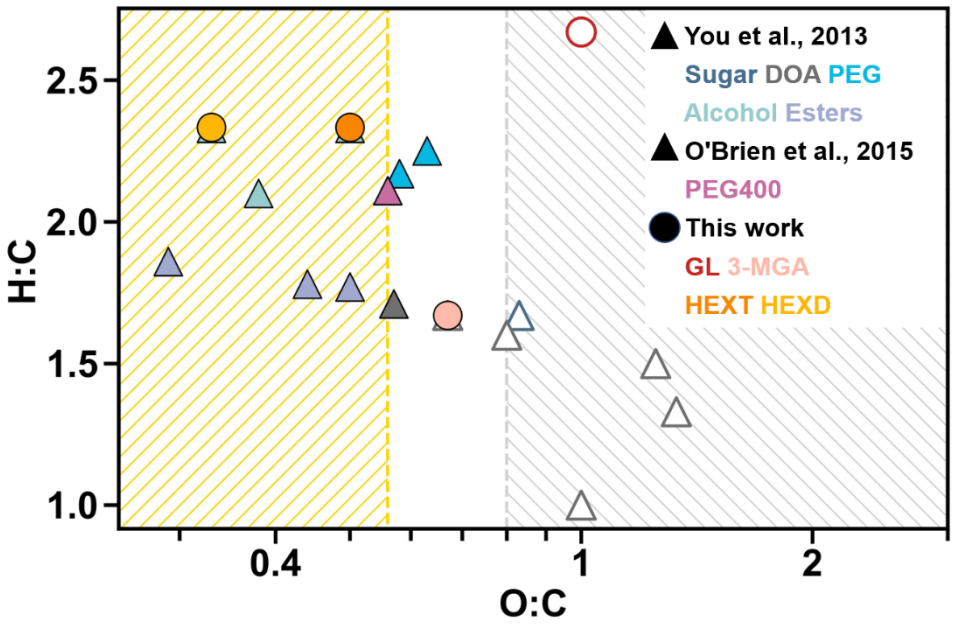

Figure S4. Van Krevelen Diagram for the mixed organic/AS particles: Solid symbols indicate that LLPS was observed, while hollow symbols indicate that LLPS was not observed. Solid triangles represent dicarboxylic acids (DOA, including malonic acid, malic acid, maleic acid, glutaric acid and diethylmalonic acid), sugars (levoglucosan), esters (including diethyl sebacate, suberic acid monomethyl ester and poly diacrylate), alcohols (including 2,5-hexanediol, propylene glycol and 1,2,6-hexanetriol), PEG (including PEG200 and PEG300) obtained from You et al. (2013), and AS-PEG400 obtained from O'Brien et al. (2015).

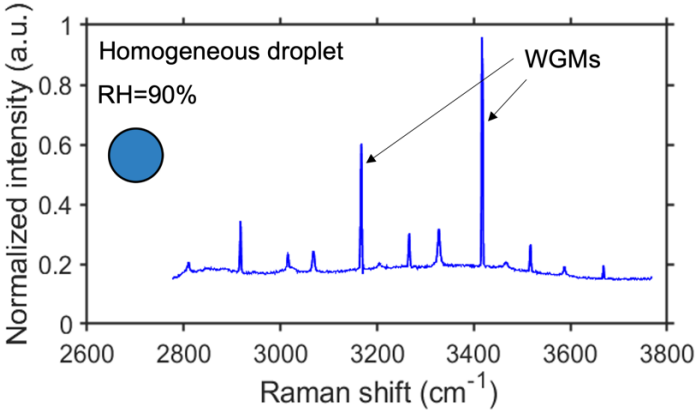

Figure S5. Raman spectra of GL microdroplets. The WGMs are marked by black arrows. The normalization of the peak is achieved by dividing it by the maximum value of the spectrum's intensity.

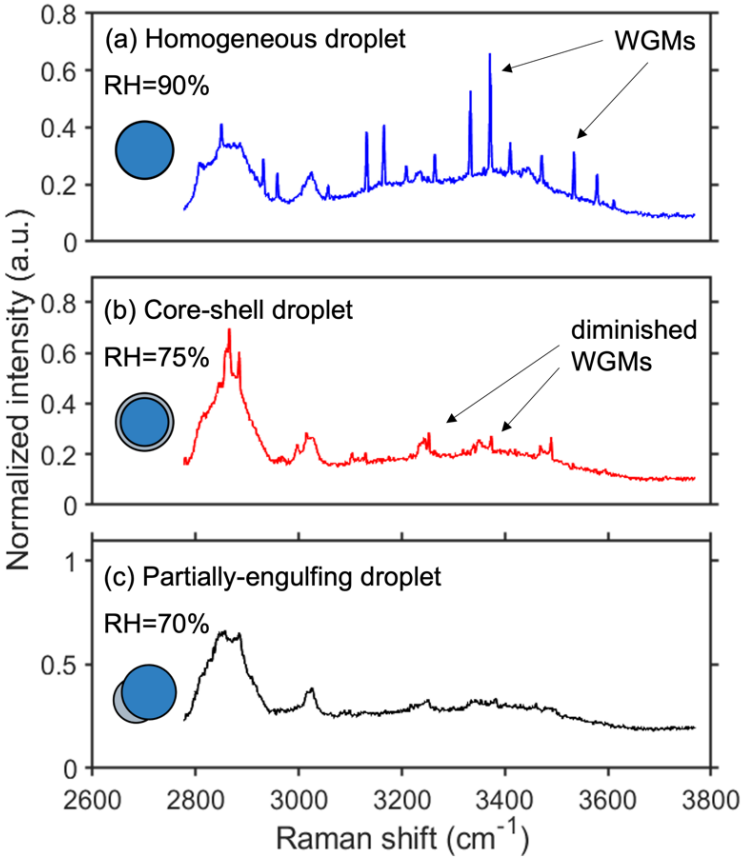

Figure S6. Raman spectra of HEXT-II microdroplets. The WGMs are marked by black arrows. The normalization of the peak is achieved by dividing it by the maximum value of its peak intensity. The origins of the spontaneous Raman peaks at 2850 and ~3050 cm^{-1} are vibration of C-H and N-H.

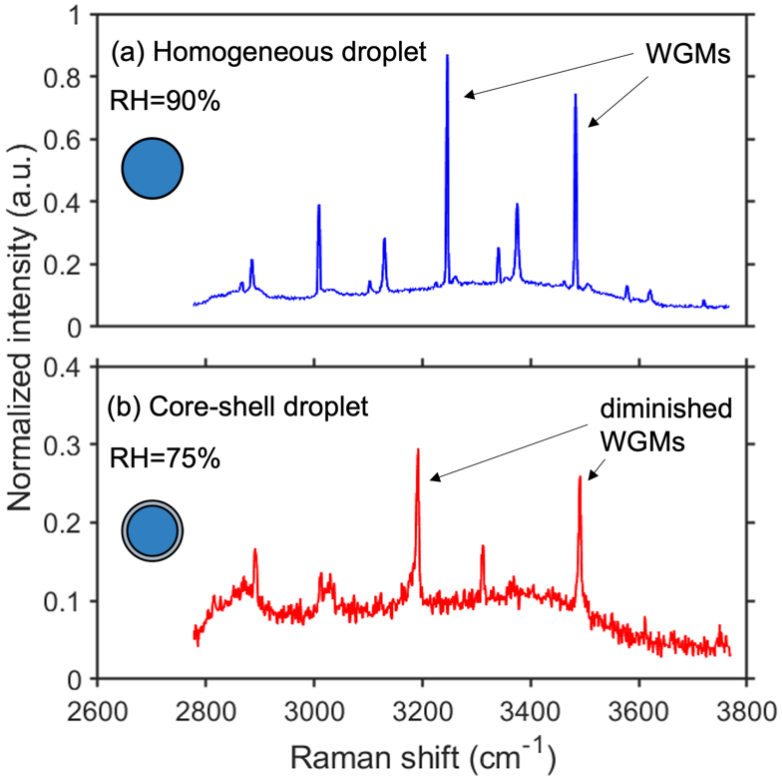

Figure S7. Raman spectra of HEXD-V microdroplets. The WGMs are marked by black arrows. The normalization of the peak is achieved by dividing it by the maximum value of its peak intensity. The origins of the spontaneous Raman peaks at 2850 and ~3050 cm^{-1} are vibration of C-H and N-H.

Table S1. Purity and suppliers of the compounds used in this study.

Compounds	Purity	Supplier
GL	99.5%	Meryer
3-MGA	99.0%	Macklin
HEXT	99.0%	TCI
HEXD	99.0%	Heowns Biochem LLC
AS	analytical reagent, >99%	Sinopharm chemical reagent
SA	analytical reagent, >99%	Sinopharm chemical reagent
NaOH	analytical reagent, 98.0%	Sinopharm chemical reagent

Table S2. Detailed SRH information of 3-MGA/AS system studied, as well as initial diameter, separation diameter (SD), separation refractive index (SRI), MRH, mixing diameter (MD), and mixing refractive index (MRI) data. Meanwhile, the last column presents the morphology of droplets when the LLPS occurred, core shell structure (CS) or partially-engulfed struture (PE).

Initial pH	Initial Dp (μm)	SRH (%)	SD (μm)	SRI (λ=650 nm)	MRH (%)	MD (μm)	MRI (λ=650 nm)	Morphology
0.48	9.86	69.5	6.02	1.576	83.5	6.82	1.540	CS
	12.08	69.8	8.45	1.454				PE
1.19	9.85	75.9	6.05	1.570	76.3	6.04	1.571	CS
	11.85	80.7	10.66	1.398	90.5	10.61	1.399	CS
	11.99	76.4	9.32	1.394	91.4	9.30	1.399	CS
2.7	8.99	75.6	6.62	1.559	84.5	6.71	1.566	CS
	12.21	82.6	9.03	1.401	90	9.01	1.400	CS
	14.86	78.6	8.00	1.518	91.6	12.21	1.559	PE
3.7	10.28	84.7	7.04	1.518				CS
	9.37	76.3	6.34	1.563				CS
	12.97	84.6	8.32	1.394				PE
5.21	12.92	89.2	9.02	1.364	89.5	7.89	1.381	CS
	10.37	89.8	8.74	1.374				CS
	9.89	88.1	9.02	1.347				CS
6.53	13.79	92.7	10.10	1.262	87.6	7.85	1.387	CS
	13.29	90.8	9.77	1.518	91.4	7.93	1.379	CS
	14.10	90.4	9.38	1.626				CS

Table S3. Detailed SRH information of HEXT/AS system studied, as well as initial diameter, separation diameter (SD), separation refractive index (SRI), MRH, mixing diameter (MD), and mixing refractive index (MRI) data. Meanwhile, the last column presents the morphology of droplets when the LLPS occurred.

Initial pH	Initial Dp (μm)	SRH (%)	SD (μm)	SRI (λ=650 nm)	MRH (%)	MD (μm)	MRI (λ=650 nm)	Morphology
0.92	14.04	75.7	10.58	1.438	85.7	10.83	1.420	CS
	14.75	76.0	10.04	1.420				PE
	11.76	76.1	9.08	1.404				CS
2.02	11.77	76.9	9.04	1.412				CS
	13.70	75.7	8.46	1.398				CS
	13.78	73.8	9.45	1.413				CS
	12.27	79.2	9.41	1.412	81.8	9.34	1.410	CS
3.14	11.14	77.3	8.44	1.407				CS
	13.10	78.1	9.38	1.410				CS
	12.39	74.7	9.05	1.408	81.3	9.04	1.409	CS
	12.60	76.2	9.18	1.408				CS
5.11	13.96	76.8	8.90	1.394	81.9	8.52	1.412	CS
	13.48	82.2	9.00	1.383				CS
	13.14	75.9	9.55	1.411	85.9	9.56	1.412	CS

Table S4. Detailed SRH information of HEXD/AS system studied, as well as initial diameter, separation diameter (SD), separation refractive index (SRI), MRH, mixing diameter (MD), and mixing refractive index (MRI) data. Meanwhile, the last column presents the morphology of droplets when the LLPS occurred.

Initial pH	Initial Dp (μm)	SRH (%)	SD (μm)	SRI (λ=650 nm)	MRH (%)	MD (μm)	MRI (λ=650 nm)	Morphology
1.39	11.28	82.4	8.64	1.375				CS
	12.35	68.0	7.96	1.414				CS
	10.82	69.9	7.83	1.408	81.2	7.93	1.406	CS
2.03	10.18	80.1	8.05	1.390				CS
	10.24	84.0	8.81	1.376				CS
	11.19	84.2	6.85	1.380	87.3	8.83	1.392	CS
2.71	13.20	78.8	8.24	1.391	89.1	8.44	1.389	CS
	14.54	78.9	8.61	1.382	91.8	8.89	1.377	CS
	15.91	75.3	8.06	1.400	88.0	8.27	1.397	CS
3.13	10.79	81.5	8.77	1.376				CS
	11.72	80.2	9.21	1.403	89.3	9.14	1.384	CS
	10.54	81.4	8.92	1.373				CS
5.01	10.20	81.4	8.77	1.362				CS
	10.55	75.5	8.01	1.393	89.7	8.00	1.393	CS
	15.09	81.2	8.20	1.397	89.5	8.76	1.387	CS

Table S5. Vapor pressure of organic compounds used in this study

Compounds	Vapor pressure (mmHg)	Reference
GL	1.66×10^{-4} to 6.68×10^{-3}	DTXSID9020663, EPA
3-MGA	7.41×10^{-7} to 2.92×10^{-4}	DTXSID50211649, EPA
	$(6.9\pm5.2)\times10^{-6}$	Booth et al. (2010)
	$(5.5\pm2.0)\times10^{-6}$	Mønster et al. (2004)
HEXT	2.12×10^{-4} to 1.82×10^{-4}	DTXSID0041224, EPA
	$(1.5\pm0.15)\times10^{-6}$	Cotterell et al. (2010)
	$(8.7\pm0.19)\times10^{-7}$	Cai et al. (2015)
HEXD	1.51×10^{-2} to 5.27×10^{-2}	DTXSID50871000, EPA

EPA means United States Environmental Protection, https://comptox.epa.gov/ (last access: 20 April 2023).

References

Booth, A. M., Barley, M. H., Topping, D. O., McFiggans, G., Garforth, A., and Percival, C. J.: Solid state and sub-cooled liquid vapour pressures of substituted dicarboxylic acids using Knudsen Effusion Mass Spectrometry (KEMS) and Differential Scanning Calorimetry, Atmos. Chem. Phys., 10, 4879–4892, https://doi.org/10.5194/acp-10-4879-2010, 2010.

Cai, C., Stewart, D. J., Reid, J. P., Zhang, Y.H., Ohm, P., Dutcher, C. S., and Clegg, S. L.: Organic Component Vapor Pressures and Hygroscopicities of Aqueous Aerosol Measured by Optical Tweezers, J.Phys. Chem. A, 119, 704-718, https://doi.org/10.1021/jp510525r, 2015.

Cotterell, M. I., Mason, B. J., Carruthers, A. E., Walker, J. S., Orr-Ewing, A. J., and Reid, J. P.: Measurements of the evaporation and hygroscopic response of single fine-mode aerosol particles using a Bessel beam optical trap, Phys. Chem. Chem. Phys., 16, 2118-2128, https://doi.org/10.1039/C3CP54368D, 2014.

Mønster, J., Rosenørn, T., Svenningsson, B., and Bilde, M.: Evaporation of methyl- and dimethyl-substituted malonic, succinic, glutaric and adipic acid particles at ambient temperatures, Journal of Aerosol Science, 35, 1453-1465, https://doi.org/10.1016/j.jaerosci.2004.07.004, 2004.